JOURNAL OF MATERIALS SCIENCE 27 (1992) 2367–2376

Cyclic hot corrosion of Haynes 230 alloy

FEN-REN CHIEN*, RICHARD BROWN
Materials Laboratory in the Department of Chemical Engineering, University of Rhode Island, Kingston, RI 02881, USA

Cyclic hot corrosion conducted on Haynes 230 at temperatures of 871 and 1093 °C indicated that catastrophic corrosion occurred. The corrosion rate was related to the high content of tungsten and chromium in the alloy. The concept of basic and acid fluxing was applied to explain the dissolution of the protective film of Cr_2O_3 and volatile WO_3 by an Na_2SO_4-rich liquid due to the formation of Na_2CrO_4 and Na_2WO_4. As the basic melts were acidified by continuously consuming oxygen ions, plate-like crystals of Cr_2O_3 were precipitated on the free surface by conversion from Na_2CrO_4. Acid fluxing was achieved by the refractory oxide, WO_3, consuming oxygen ions. The presence of sulphur suppressed the diffusion of chromium outward to form protective Cr_2O_3. Internal chromium-rich sulphide particles were observed. It was suggested that at very low P_{O_2}, sulphur reacted with chromium to form CrS initially. As oxygen penetrated through the porous layer, the CrS was oxidized internally to Cr_2O_3.

1. Introduction

The presence of sulphur or vanadium contaminants in the ambient gases, such as sulphates or vanadates, accelerate corrosion [1–3]. Hot corrosion has been encountered in gas turbines where sulphatic deposits provide the source of sulphur. Sulphur can penetrate oxide films, and reactions are enhanced, particularly if molten sulphates are formed. Hot corrosion is especially damaging to nickel-based alloys exposed to high-sulphur partial pressures. In the case of nickel, the rate of oxidation is several orders of magnitude greater in an $SO_2 + O_2$ atmosphere than in an O_2 atmosphere [1–3]. Hocking and co-workers [1, 2, 5, 6] have studied the kinetics and mechanism of corrosion of nickel, chromium and Ni–Cr (0.1–50 at % Cr) alloys in an SO_2/O_2 mixture and indicated that NiO, Cr_2O_3, Ni_3S_2 and CrS were the main corrosion products. Besides the above-mentioned corrosion products, Cr_3S_4 was also reported by Davin and Coutsouradis [7]. Earlier experimental results indicated that pure nickel, after forming a protective oxide layer in oxygen, lost its protective oxide when exposed to an atmosphere containing SO_2 at 1000 °C [8]. Sulphur penetrated the oxide scale and formed an Ni–Ni_3S_2–NiO ternary eutectic which resulted in extensive grain-boundary attack of the metal. A different mechanism for the formation of the eutectic liquid has been reported by Sidky and Hocking [1, 2]. The experimental results, for nickel-based ternary alloys in an SO_2/O_2 atmosphere, indicated that the corrosion rates at 700 °C were much greater than those at 900 °C due to the inclination to form an Ni–Ni_3S_2 eutectic liquid with a formation temperature at 637 °C. At 900 °C, neither Ni_3S_2 nor CrS forms as readily as at 700 °C. If a continuous liquid phase is formed at the scale–metal interface, scale–metal adhesion is greatly impaired and this leads to disastrous spalling of the scale.

The mechanism of Na_2SO_4-induced corrosion at high temperatures [9–15], above the 884 °C melting temperature of Na_2SO_4, has been extensively studied. Luthra and Shores [9] have shown that Co-30Cr and Ni–30Cr alloys coated with Na_2SO_4 formed Na_2SO_4–$CoSO_4$ and Na_2SO_4–$NiSO_4$ eutectic liquid when exposed to O_2–SO_2–SO_3 environments containing sufficient SO_3. Because $NiSO_4$, $CoSO_4$ and $CrSO_4$ are water soluble, they were seldom detected by metallographic examination. Because the rapid sulphation of cobalt and nickel oxides on the surface of the alloys prevent the formation of protective Cr_2O_3 films, high corrosion rates were found. It was also concluded that the combination of various factors involved in the sulphation reaction and the enhanced tendency to form a protective Cr_2O_3 film at high temperatures results in a maximum in the corrosion rates at about 650–750 °C. However, in the absence of SO_2 (or SO_3) environments, the hot corrosion mechanisms are totally different from those described, because not enough P_{SO_3} is available to form $NiSO_4$ or $CoSO_4$.

It is generally accepted that hot corrosion of alloys used in gas turbines is caused by the deposition of Na_2SO_4 resulting from the ingestion of salts in the engine and sulphur from the combustion of fuel [16, 17]. The objective of this research was to investigate the mechanisms of hot corrosion in Haynes 230 alloy. In order to simulate the presence of sulphur contaminants, the sample was coated with Na_2SO_4. The concept of basic and acidic fluxing is applied to explain the formation of Na_2CrO_4 and

*Present address: Division of Engineering, Brown University, Providence, RI 02912, USA.

0022–2461

WO_3/Na_2WO_4 which is a disastrous product when formed during hot corrosion.

2. Experimental procedure

The samples for hot corrosion of Haynes 230 were small discs of 1.25 cm diameter and 0.3 cm thick. The chemical composition for Haynes 230 has been described previously [18]. Before Na_2SO_4 coating, the surface of the discs were wet ground on silicon carbide paper down to 600 grit and cleaned in acetone. Na_2SO_4 has a high solubility in water (0.28 g cm^{-3}) at room temperature. Saturated Na_2SO_4 solution in water was sprayed by an air brush on surfaces preheated to 200 °C for a coverage of 2.5 ± 0.2 mg cm^{-2} for the samples. The microstructure of the Na_2SO_4-sprayed surface is shown in Fig. 1, while its EDS spectrum is shown later in Fig. 5a. The same furnace and environment as for cyclic oxidation was employed, which has been described previously [18]. The period of the cycle was 30 min in the furnace and 5 min at ambient conditions. The furnace was set at two different operating temperatures; 871 and 1093 °C. Several short-term tests were conducted to examine the corrosion mechanisms. Consequently, comparable tests were done over an extended exposure period of 150 h.

After hot corrosion, the disc samples were cross-sectioned by a diamond saw and mounted in epoxide resin. Because most of the products from the reaction with Na_2SO_4 are water soluble, kerosine was used for the following metallographic examination instead of water. The mounted specimens were ground on SiC paper down to 1200 grit, then polished to a 0.3 μm alumina paste finish. When etching was required, the etching solution which was made up of 30 ml HCl, 10 ml HF and 10 ml HNO_3 was used. A scanning electron microscope (SEM) was employed to observe the crystal morphology and microstructure of the sample surfaces and the cross-sections. In addition, energy dispersive X-ray analysis (EDS) was conducted to identify the composition of the surface and additional layers formed during the test.

3. Results

3.1. Weight change behaviour

The weight change behaviour of the discs with 0.25 mg cm^{-2} Na_2SO_4 coatings as a function of exposure time and temperature are shown in Fig. 2. For a nonsulphate-coated sample, only a weight gain was found under the same exposure conditions [18], indicating the severity of attack by the sodium sulphate. A closer examination of the weight change curve, Fig. 2, indicated that initially, the weight increased due to metal diffusing outward to the surface to form metal oxide films. During the following stage, Na_2SO_4 dissolved or reacted with the initially formed protective films. With the oxide films destroyed or altered, their protective nature stopped. Consequently, the sample lost weight due to the scale spalling and because of the vaporization of Na_2SO_4 ($Na_2O_{(g)} + SO_{3(g)}$). During 871 and 982 °C cyclic exposure, no obvious spalling was observed. At 1093 °C, during cyclic exposure, large pieces of surface scale spalled from the discs' edges and were collected for further microscopic examination. Additionally, many particles were noted separating from the scale surface when the discs were cooling in air. This observation of scale failure may be used to explain their non-protective nature during thermal cycling.

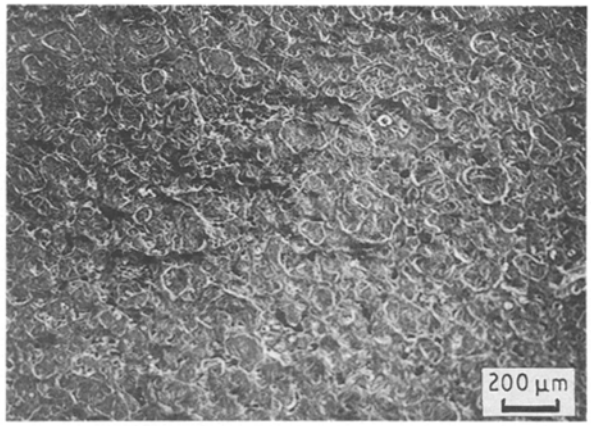

Figure 1 Microstructure of the original Na_2SO_4-sprayed surface.

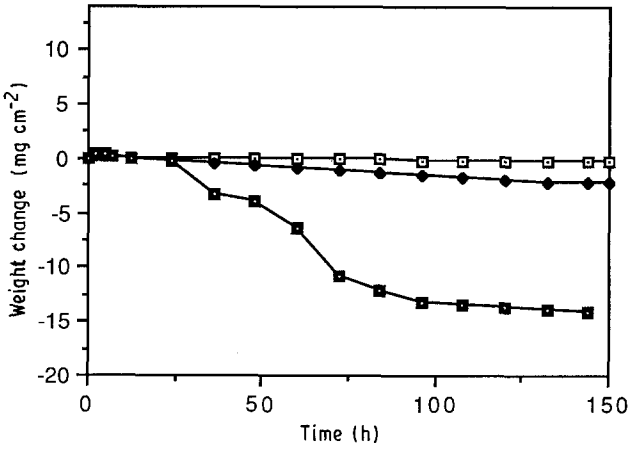

Figure 2 Weight change behaviour of cyclic hot corrosion for 150 h. (□) 871 °C, (◆) 982 °C, (■) 1093 °C.

3.2. Surface microstructure

3.2.1. 871 °C

The melting temperature of Na_2SO_4, 884 °C, is slightly higher than the thermal exposure temperature, 871 °C. During the first 6 h testing, the surface was dry, but gradually a very thin liquid layer covered the surface. Because the thermal treatment temperature was so close to the melting temperature of Na_2SO_4, the formation of a liquid phase may have occurred. In addition, a solid state reaction, such as a eutectic reaction for the scales (i.e. Cr_2O_3) and Na_2SO_4 may occur or the molten Na_2SO_4 reacted with the scales, i.e. [19, 20]

$$Cr_2O_{3(s)} + 3/2O_2 + 2Na_2SO_{4(l)} = 2Na_2CrO_{4(l)} + 2SO_{3(g)} \quad (1)$$

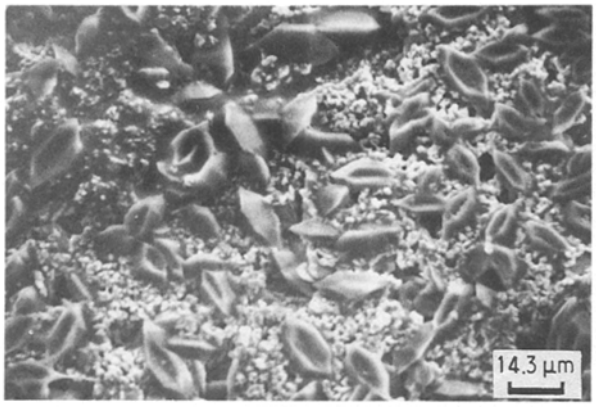

Figure 3 Surface microstructure after 150 h cyclic exposure at 871 °C.

After 150 h thermal treatment, the surface microstructure was as shown in Fig. 3. The large crystals were Na_2SO_4 which recrystallized under high-temperature ageing. The porous agglomerations were chromium-rich with nickel oxides. EDS analysis for the average surface composition is shown below in Fig. 5b.

3.2.2. 1093 °C

The discs coated with Na_2SO_4 were thermally treated at three different exposure times: 16, 70 and 150 h. The surface microstructures after the three different exposure times are shown in Fig. 4a–c. The surface after 16 h exposure was covered with a liquid layer in which particles were dispersed. EDS for the average composition of the surface is shown in Fig. 5c. EDS analysis indicated that the liquid phase was both tungsten- and chromium-rich with high sodium content, and the isolated particles were nickel-rich crystals. Only a small amount of sulphur was detected. These results were consistent with the basic fluxing theory. The initially formed Cr_2O_3 scale was dissolved in molten Na_2SO_4. Furthermore, WO_3, which accumulated in the molten liquid, could not escape by means of vaporization. According to the reactions [19, 20]

$$Cr_2O_{3(s)} + 3/2O_2 + 2Na_2SO_{4(l)} = 2Na_2CrO_{4(l)} + 2SO_3 \quad (2)$$

$$WO_{3(s)} + Na_2SO_{4(l)} = Na_2WO_{4(l)} + SO_3 \quad (3)$$

of the chromium, tungsten and nickel oxides capable of being formed, only nickel-rich oxides, which dispersed as small crystals in the liquid phase, could not be dissolved by fluxing. The reaction product $SO_{3(g)}$ either diffused into the alloy or escaped to the air, which is why only a low sulphur content was detected on the surface.

After 70 h thermal exposure, plate-like crystals covered the surface. The plate-like crystals were highly chromium-rich, and they precipitated from the molten phase. The surface average composition is shown in Fig. 5d. The precipitation mechanism will be discussed in the next section.

After 150 h exposure, some spalling traces were apparent, Fig. 4c. Some spalled films were collected for further examination. EDS analysis identified that the average surface composition, in Fig. 5e, was mainly chromium-rich with some nickel present.

3.3. Cross-sectioned microstructure

3.3.1. 871 °C

The microstructure of the scale after 54 h exposure is shown in Fig. 6. The externally exposed top porous layer was a Na_2SO_4-rich compound mixed with small amounts of Cr_2O_3. An intermediate layer existed between the top porous layer and the matrix which contained chromium-rich oxides marked "A", Fig. 6. Other areas of interest were large attacked areas connected to grain boundaries intersecting the surface

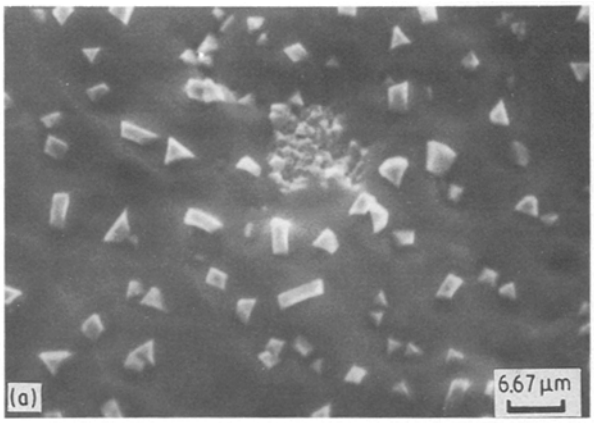

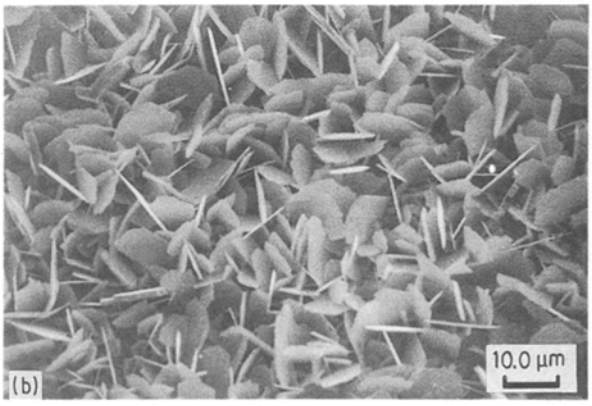

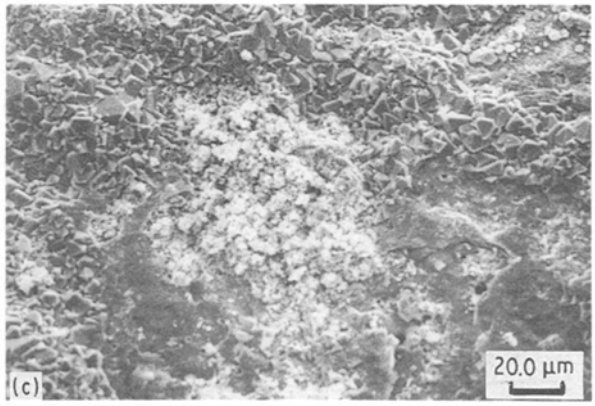

Figure 4 Surface microstructures after cyclic exposure at 1093 °C: (a) 16 h exposure, (b) 70 h exposure, (c) 150 h exposure.

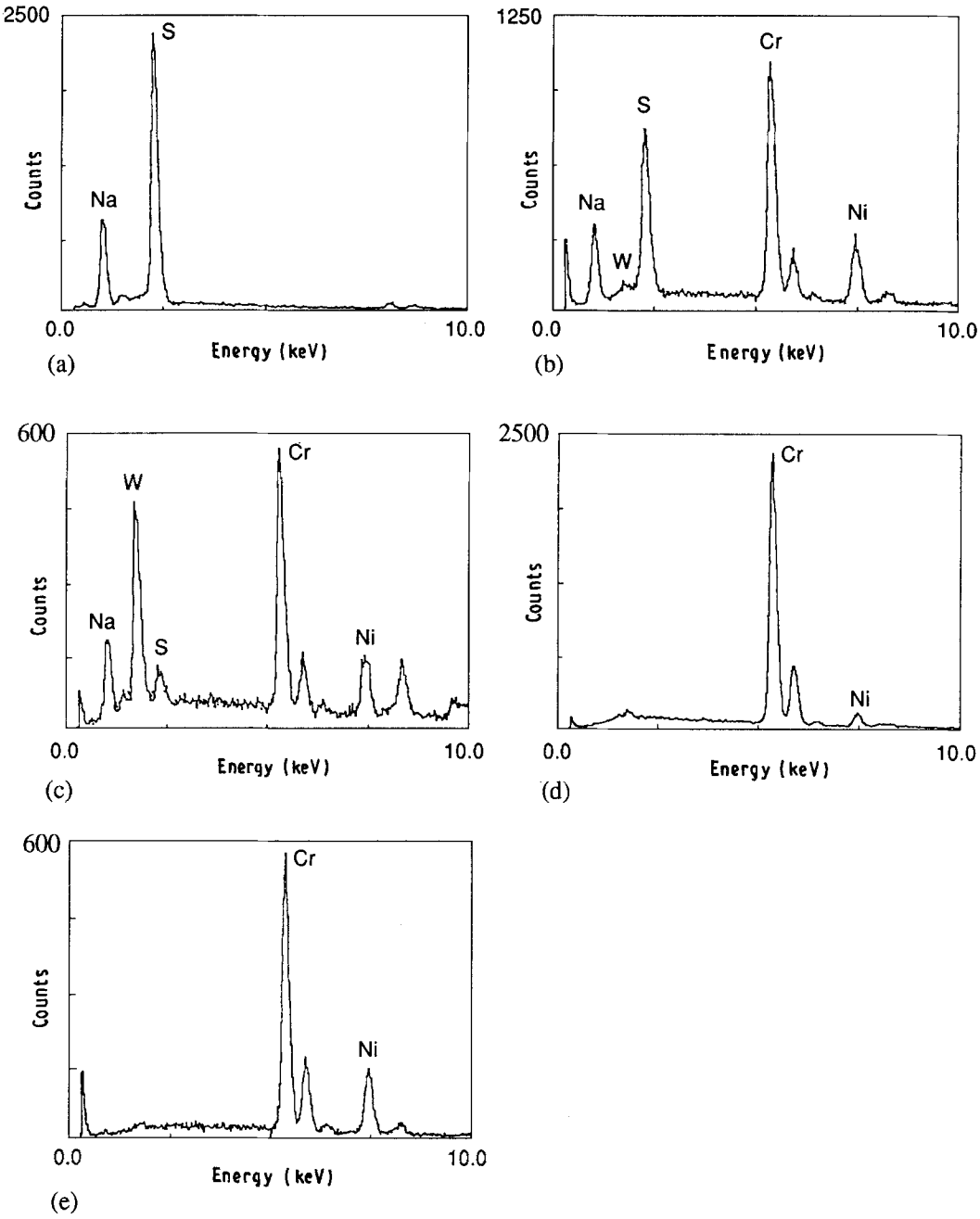

Figure 5 EDS analysis of the surface compositions before and after cyclic exposure with Na_2SO_4 coating: (a) as-Na_2SO_4 sprayed, (b) 871 °C, 150 h exposure, (c) 1093 °C, 16 h exposure, (d) 1093 °C, 70 h exposure, (e) 1093 °C, 150 h exposure.

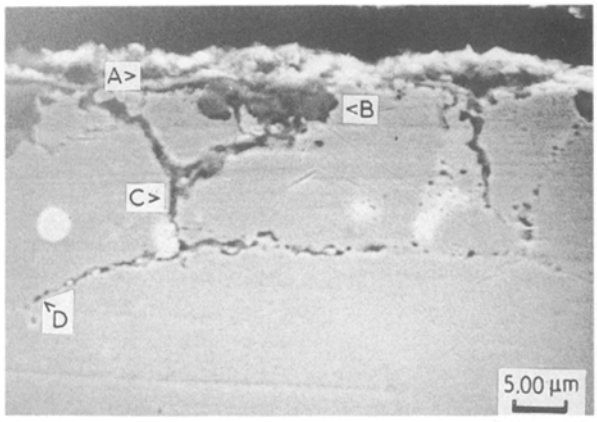

Figure 6 The cross-sectioned microstructure after 54 h cyclic exposure at 871 °C.

marked "B", and the upper portion of the grain boundaries marked "C". Both regions were identified as chromium-rich oxides, but their formation mechanisms were believed to be different from the development of the external chromium-rich oxide scale. It is apparent that the grain boundary appearance, in Fig. 6, indicated attack into the substrate and was controlled by the gas species, i.e. O_2 or SO_3, diffusing along grain boundaries into the alloy. This mechanism is different from the selective surface oxidation of chromium when no sulphate is present. In the substrate, little sulphur could be detected by EDS in the areas marked "B" and "C". The sulphur was found to be concentrated at the front of attacked grain boundaries, growing into the substrate away from the free surface, marked "D" in Fig. 6. It is suggested that the

deepest grain-boundary attack was from sulphide formation. This indicated that the diffusion ability and solubility of sulphur into the alloy are stronger than oxygen. Therefore, it is suggested that the areas and the upper grain boundaries noted, which were identified as chromium-rich oxides, were originally sulphide compositions and later transformed to oxide as the sulphur continued moving internally on grain boundaries. As the scale broke down, the oxygen might diffuse into the alloy and react with the initially formed sulphides

$$2CrS + 3O_{(diss)} = Cr_2O_3 + 2S_{(diss)} \quad (4)$$

$$NiS + O_{(diss)} = NiO + S_{(diss)} \quad (5)$$

The released $S_{(diss)}$ could react with substrate alloy, especially along the grain boundaries because they can accommodate more $S_{(diss)}$. Because Cr_2O_3 is thermodynamically more stable than NiO, usually Cr_2O_3 and NiO cannot coexist at the same time. Therefore, the NiO might be replaced by chromium

$$3NiO + 2Cr = 3Ni + Cr_2O_3 \quad (6)$$

with nickel back into the alloy [21]. This explained why the areas marked "B" and the new surface-attacked grain boundaries were chromium-rich oxides.

3.3.2. 1093 °C

The etched microstructure of a sample after 4 h exposure is shown in Fig. 7. There was a very thin top layer covering the surface. Below this top layer existed a different thicker second-phase layer. EDS analysis identified the top layer as essentially chromium-rich oxides and the second layer was predominantly a nickel-rich region. The reason for the existence of the chromium-rich top layer was that the initially formed Cr_2O_3 layer had not been totally dissolved in the molten Na_2SO_4. As the liquid phase diffused through the porous external layer, especially along the grain boundaries, the chromium and tungsten segregated to form Na_2CrO_4 and Na_2WO_4. These chromate and tungstenate compounds are soluble in water. After etching, several big cavities appeared along the grain boundaries and the top/second layer interface. These cavities were supposed originally to have been filled by the Na_2CrO_4 and Na_2WO_4. Owing to segregation of chromium and tungsten from nickel, the nickel-rich region was developed.

As the exposure time was increased to 16 h, portions of the nickel-rich region were oxidized and thereby a row of nickel-rich islands was developed marked "E", Fig. 8, at the position of the nickel-rich region initially. Because chromium and nickel were consumed near the surface, the Al_2O_3 concentration increased. As the modified Na_2SO_4 was in a basic condition, Al_2O_3 dissolves in the modified liquid according to the reaction [19, 20]

$$Al_2O_3 + O^{2-} = 2AlO_2^- \quad (7)$$

As the modified liquid was acidified again because of the consumption of O^{2-}, the chromate and aluminate ions oxidized again. Therefore, the layer marked "F" in Fig. 8 just above the matrix was aluminium- and chromium-rich.

There was some indirect evidence to show that Na_2CrO_4 and Na_2WO_4 actually existed in the scales, which is present in the structure shown in Fig. 9. Na_2CrO_4 and Na_2WO_4 are soluble and can absorb humidity from the air to recrystallize. Therefore, these chromate and tungstenate crystal shapes were subject to change with exposed time in air. It is interesting

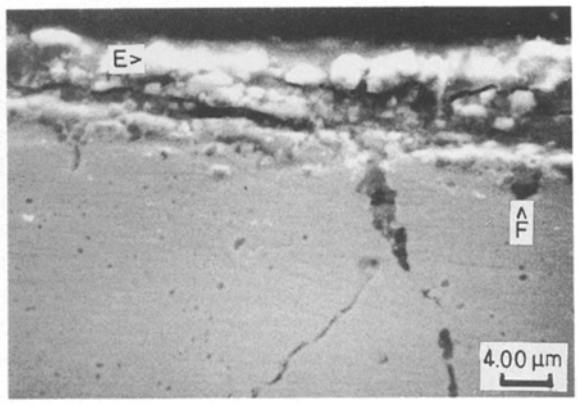

Figure 8 The cross-sectioned microstructure after 16 h cyclic exposure at 1093 °C.

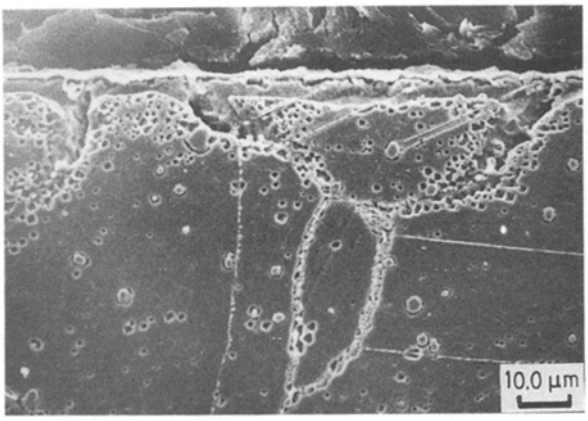

Figure 7 The cross-sectioned microstructure after 4 h cyclic exposure at 1093 °C.

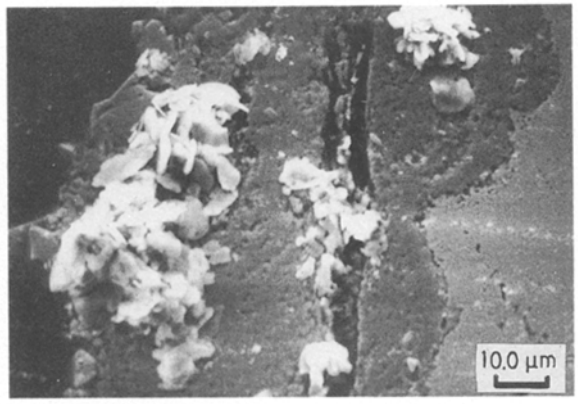

Figure 9 The microstructure after 16 h cyclic exposure at 1093 °C: the melt within the scale absorbed water from humid air to recrystallize. The crystal morphology is subject to change with time.

that the compositions of the crystals were not the same everywhere. In Fig. 9, the plate-like crystals growing at the outer layer have a higher concentration of Na_2CrO_4. Meanwhile, the crystals growing near the matrix have a higher concentration of Na_2WO_4. These results possibly may be evidence that the accumulation of WO_4^{2-} played a major role in the mechanism of the hot corrosion in this study. The presence of liquid phases might provide short-circuit paths for either oxygen or sulphur, and accelerate cracking as well. Because the liquid was developed in the attacked region and it provided the accelerated path for the diffusion of oxygen or sulphur, chromium was prevented from diffusing outward to form the protective film.

For some locally attacked areas, tungsten-rich oxides were found at the attacking front, marked "G" in Fig. 10. It suggested that the tungsten carbides could be oxidized easily. The acidic fluxing by WO_3/Na_2WO_4 can be established because WO_3 may consume O^{2-}. The newly formed Cr_2O_3 could be dissolved in this acidic fluxing

$$Cr_2O_3 = 2Cr^{3+} + 3O^{2-} \quad (8)$$

$$WO_3 + O^{2-} = WO_4^{2-} \quad (9)$$

Therefore, under the acidic fluxing, the overall reaction is

$$Cr_2O_3 + 3WO_3 = 2Cr^{3+} + 3WO_4^{2-} \quad (10)$$

The metal cations (Cr^{3+}) diffused to the outer zone of the melt where they were reoxidized by a higher oxygen potential.

However, indications were found for solubility of sulphur in the alloy. In Figs 10 and 11, a large number of small internal sulphide particles were found, marked "H". EDS analysis indicated that the internal particles were chromium-rich sulphides with some nickel content. No aluminium was detected, which implied that the free energy for the formation of chromium sulphide is lower than aluminium sulphide. In comparison, under cyclic oxidation in air at 1093 °C, some internal aluminium-rich particles were found [18].

After 150 h exposure, a large amount of scales spalled from the surface. In Fig. 12, a small piece of film is seen spalling from the substrate. Apparently, the material spalling in Fig. 12 had two different phases, one was on the exposed surface which was composed of large crystals, and the other phase at the scale/alloy interface was a porous area. EDS analysis showed that the large crystals were nickel-rich oxides. Their precursors might be the nickel-rich islands shown in Fig. 8 previously. The porous area was chromium-rich oxide. The area marked "I" in Fig. 12a within the substrate alloy had the same composition as the spalling material. It indicated that the chromium was

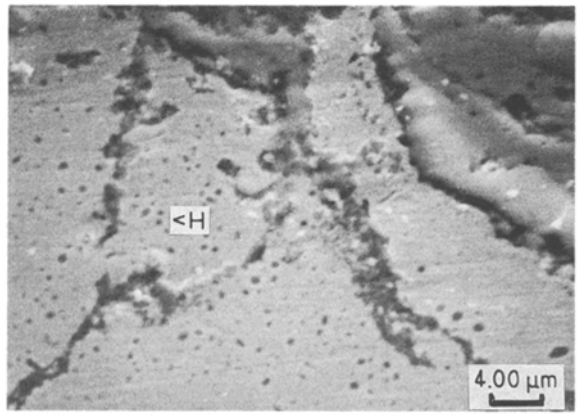

Figure 11 Formation of internal chromium-rich sulphide particles along the attacked grain boundaries after 16 h cyclic exposure at 1093 °C.

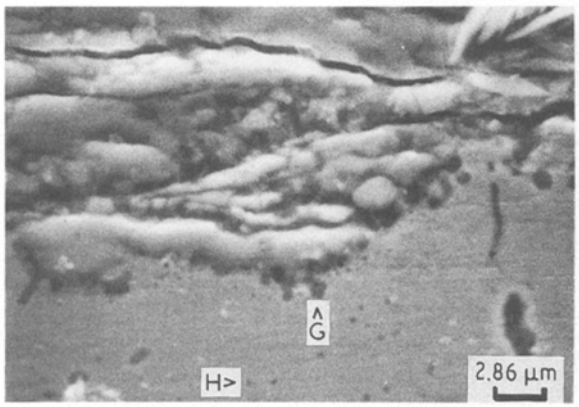

Figure 10 Locally attacked area after 16 h cyclic exposure at 1093 °C. The front tip marked "G" is a tungsten-rich oxide with some chromium content.

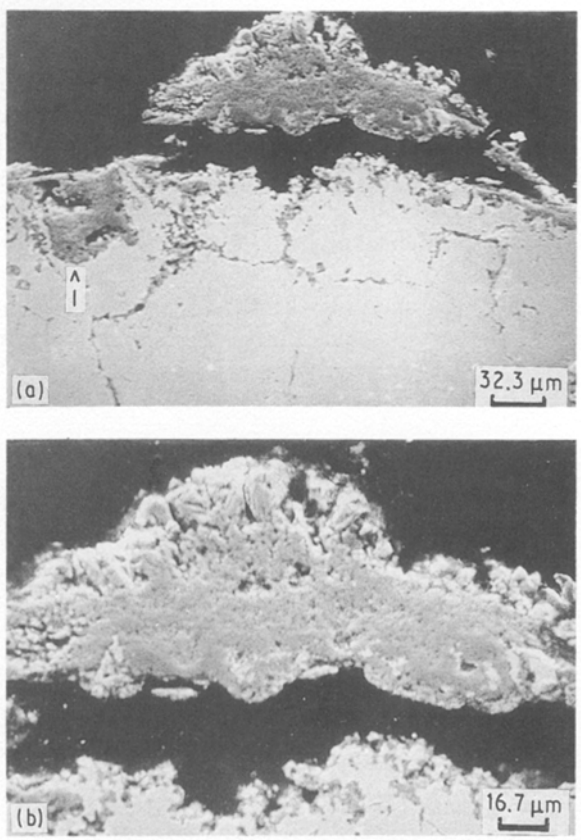

Figure 12 (a) A small piece of film spalling from the substrate after 150 h cyclic exposure at 1093 °C. (b) A higher magnification view of the spalling film.

prevented from uniformly diffusing outward to form a protective film. This mechanism will be discussed further in the next section.

An interesting feature was that the attacked grain boundaries were sulphur free after 150 h exposure. Most of the grain boundaries contained highly chromium-rich oxides. Only a few of them at the deeper regions had highly aluminium-rich oxides. No sulphur was detected in the attacked grain boundaries, and it could be due to the extensive oxidation from chromium sulphides being oxidized to chromium oxides. The reason for the formation of aluminium-rich oxide in the deeper grain boundaries was due to the occurrence of intergranular oxidation which has been described in the previously of the cyclic oxidation in air [18].

4. Discussion

The proposed corrosion mechanisms based on the experiment of 1093 °C cyclic thermal exposure are described. Most fluxing mechanisms were invoked from the phase stability diagrams. Generally, Cr_2O_3, Al_2O_3 and NiO are the primary oxides for high-temperature alloys and they all exhibit amphoteric behaviour in Na_2SO_4 [19]. WO_3 only favours basic fluxing. Fryburg *et al.* [19] have constructed the phase stability diagrams for the Cr–, Al– and Ni–O–S systems, superimposed on a diagram for the Na–O–S system for a temperature of 900 °C. Although the experimental temperature is higher than the temperature (900 °C) of the available phase stability diagrams, these still are good reference for the evaluation of fluxing mechanisms.

In hot corrosion tests, an assumption is made that the corrosion starts from "neutral" Na_2SO_4 [19], which implies that in the molten Na_2SO_4 the activities of Na_2O and SO_3 are identical, $\log a_{Na_2O} = \log P_{SO_3}$, at "neutral" Na_2SO_4. In this study, the experiment was operated at air atmosphere, therefore $\log P_{O_2} \approx -0.7$. Under such conditions, it is evident that in the Cr–, Al– and Ni–O–S systems, NiO is a very stable phase; Al_2O_3 is not a very stable phase and basic fluxing may proceed if the system is shifted slightly to more basic; Cr_2O_3 can react with the molten Na_2SO_4 forming soluble chromate (CrO_4^{2-}) and liberate SO_3. The natural protective oxide in Haynes 230 alloy is Cr_2O_3. Thus, as soon as the Cr_2O_3 layer forms, it is unstable as Cr_2O_3 inclines to be dissolved in the molten Na_2SO_4.

A schematic illustration for the proposed hot corrosion mechanisms is shown in Fig. 13a–d. The corrosion processes were separated into four distinct stages.

4.1. Stage A – induction period

Immediately upon bringing the test discs to temperature, chromium-rich oxides form on the surface as shown in Fig. 7. In comparison with the weight change behaviour in Fig. 2, it is evident that the weight increased only at the initial stage. This implied the oxidation occurred immediately as the discs were brought to the temperature. At the same time, the surface tungsten carbides and tungsten in the alloy may be oxidized as WO_3. The oxides developed of Cr_2O_3 and WO_3 react with the molten Na_2SO_4 forming soluble chromate and tungstenate while liberating SO_3 as follows [19, 20]:

$$Cr_2O_3 + 3/2O_2 + 2Na_2SO_{4(l)} = 2Na_2CrO_{4(l)} + 2SO_{3(g)} \quad (11)$$

$$WO_3 + Na_2SO_{4(l)} = Na_2WO_{4(l)} + SO_{3(g)} \quad (12)$$

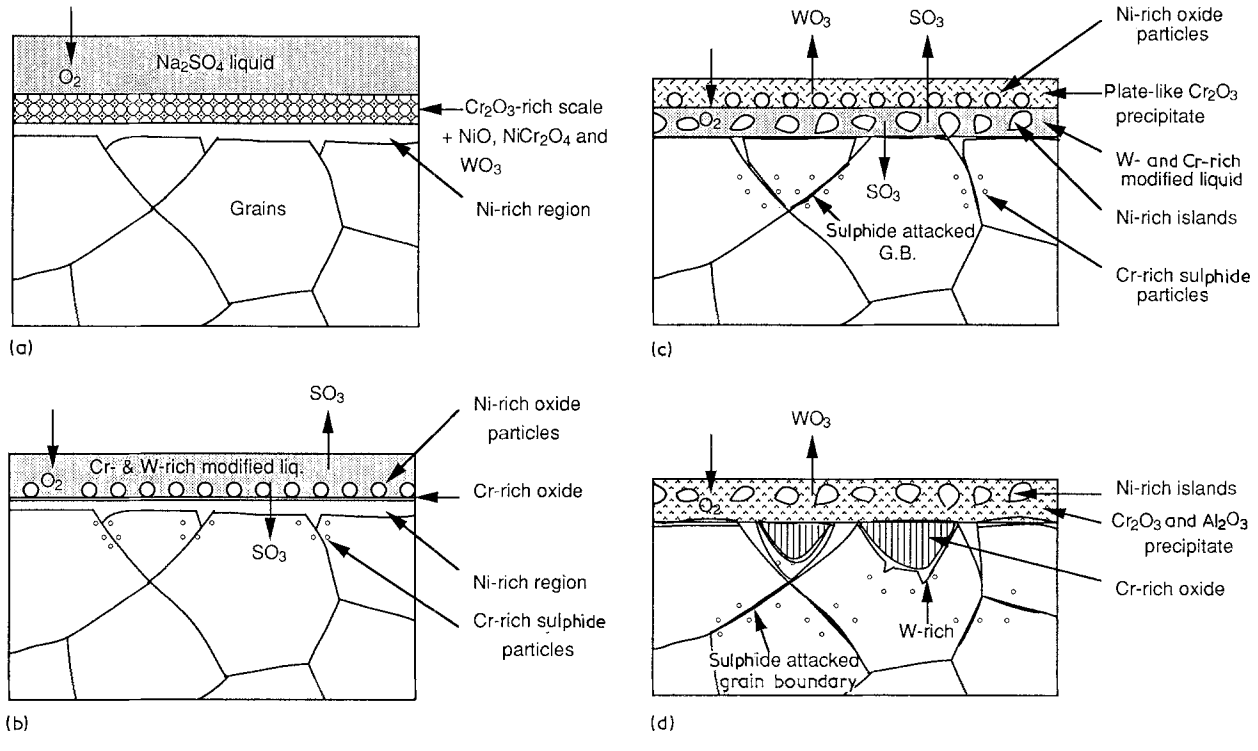

Figure 13 A schematic illustration of the proposed corrosion mechanisms: (a) Stage A, (b) Stage B; (c) Stage C; (d) Stage D.

It should be noted that these reactions consume oxygen ions, increasing the acidity of the modified liquid. It is also important that the refractory oxide WO_3 is stabilized as $Na_2WO_{4(l)}$ and the vaporization rate is reduced, adjusting the fluxing. The reactions are shown schematically in Fig. 13a.

4.2. Stage B – consumption of oxygen ions predominating the fluxing

Initially, chromium was selectively oxidized from the surface alloy. However, some nickel was oxidized at the same time. The molten "neutral" Na_2SO_4 dissolved Cr_2O_3 and WO_3 and liberated SO_3 as described above, but cannot dissolve NiO nor nickel-rich oxides. Therefore, only these nickel-rich oxides survived on the top surface. The reaction product $SO_{3(g)}$ may diffuse into the alloy, and it can react with substrate metal directly by oxidation or sulphidation depending on oxygen partial pressure, Fig. 13b.

High P_{O_2}

$$Ni + SO_3/O_2 = NiO + SO_2 \quad (13)$$

$$2Cr + 3SO_3/O_2 = Cr_2O_3 + 3SO_2 \quad (14)$$

Low P_{O_2}

$$Ni + SO_3/O_2 = NiS + 3/2O_2 \quad (15)$$

$$Cr + SO_3/O_2 = CrS + 3/2O_2 \quad (16)$$

In this study, evidence, i.e. Figs 6 and 9, indicated that the appearance of sulphur below the surface prevents chromium from diffusing outward to form a protective film. However, it is very likely that the reaction occurs due to the sulphur diffusing into the substrate, probably because sulphur has higher penetration ability than oxygen. Therefore, a nickel-rich region (chromium-depleted region) was maintained after an initially short stage of selective oxidation of chromium, as shown in Fig. 7. Overall, at this stage, consumption of oxygen ions predominates the fluxing, which creates chromate and tungstenate, resulting in an acidic environment.

4.3. Stage C – change of acidic to basic melt then return to acidic again

Sulphidation and/or oxidation of the underlying alloy may occur because SO_3 is liberated from the previous basic fluxing. It is suggested that the reaction may be favourable to oxidation due to high P_{O_2}, resulting from the high penetration rate of oxygen through the porous outer layer which is covered with liquid. Thus, the nickel-rich region was oxidized according to the reactions

$$Ni + SO_3/O_2 = NiO + SO_2/O_2 \quad (17)$$

$$2Cr + 3SO_3/O_2 = Cr_2O_3 + 3SO_2/O_2 \quad (18)$$

$$2Al + 3SO_3/O_2 = Al_2O_3 + 3SO_2/O_2 \quad (19)$$

$$W + SO_3/O_2 = WO_3 + S_{(diss)}/O_2 \quad (20)$$

These reactions consume acid (SO_3), and the melt becomes basic again. Consequently, basic fluxing of Al_2O_3, Cr_2O_3 and WO_3 may take place again, but nickel-rich oxides are not dissolved and are stable. As the basic melt migrates across the nickel-rich region, a row of nickel-rich oxides appears at the original place of the nickel-rich region, as shown in Figs 8 and 13c. Eventually, after a period of consumption of O^{2-} in basic fluxing, the melt is acidified again. Some reports [18, 19] indicated that the acidic melt was mainly achieved by WO_3 consuming O^{2-} to form WO_4^{2-}. At this stage, large amounts of Na_2CrO_4 exist in the melt. The stable phase, in the phase diagram, shifts from Na_2CrO_4 to Cr_2O_3. Thus, the plate-like Cr_2O_3 are precipitated on the free surface, as shown in Fig. 4b.

There is indirect evidence to show that Na_2WO_4 actually existed within the scales. During the test, after 30 h exposure some spalled films were collected. The surface adjacent to the substrate surface was originally covered with the melt, which was the Na_2WO_4-rich melt. As Na_2WO_4 absorbed humidity from the air, it crystallized into the large clusters marked "J" in Fig. 14. In Fig. 14, the substrate underneath the Na_2WO_4-rich crystals was nickel-rich oxide marked "K". This is consistent with the phase stability diagram which shows NiO is a stable phase. It is also noted that initially the top melt was Na_2CrO_4-rich, and the melt within the scales was Na_2WO_4-rich. It indicated that WO_3 cannot escape by vaporization and accumulates within the scale as WO_4^{2-}. In other words, the available oxygen ions will be exhausted by WO_3 transforming to Na_2WO_4, resulting in an acidic melt which will not return to a basic melt. Although

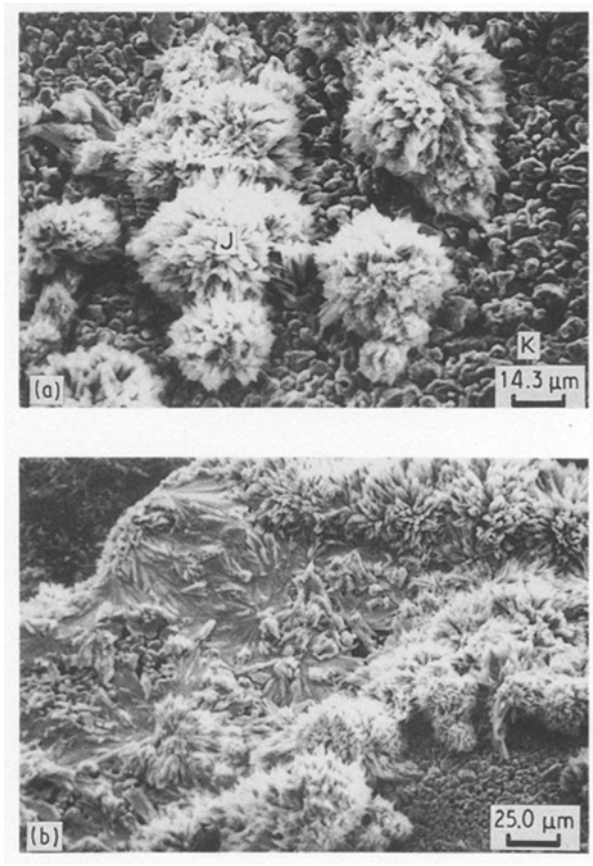

Figure 14 (a, b) The melt underneath the spalling film recrystallized in air.

the melt is acidified, the acid fluxing may or may not occur depending on P_{O_2} and the residual P_{SO_3}. If P_{O_2} at the position close to the substrate metal is very low, the possible reactions in this acidified system are

$$Cr + SO_3 = CrS + 3/2O_2 \quad (21)$$

$$Al + 3SO_3 = Al_2O_3 + 3SO_2 \quad (22)$$

The formation of Al_2S_3 maybe needs a much lower P_{O_2} value. As the scale broke down, oxygen could diffuse into the alloy and react with the initially formed sulphides

$$2CrS + 3O_{(diss)} = Cr_2O_3 + 2S_{(diss)} \quad (23)$$

Therefore, if the melt is extremely acidic, the acidic fluxing of Cr_2O_3 and Al_2O_3 may proceed [19, 20]

$$Cr_2O_3 = 2Cr^{3+} + 3O^{2-} \quad (24)$$

$$Al_2O_3 = 2Al^{3+} + 3O^{2-} \quad (25)$$

and WO_3 may consume O^{2-}

$$WO_3 + O^{2-} = WO_4^{2-} \quad (26)$$

Under the acidic fluxing, the overall reactions are

$$Cr_2O_3 + 3WO_3 = 2Cr^{3+} + 3WO_4^{2-} \quad (27)$$

$$Al_2O_3 + 3WO_3 = 2Al^{3+} + 3WO_4^{2-} \quad (28)$$

The metal cations (Cr^{3+} and Al^{3+}) may diffuse to the outer zone of the melt where they are reoxidized by a higher oxygen potential. Although aluminium concentration in Haynes 230 is only 0.3 wt %, at this stage a noticeable aluminium concentration accumulated at the layer near the substrate metal.

There is evidence to show that CrS is more stable than NiS. In Fig. 11, internal chromium-rich sulphide particles have been observed. They dispersed within the grains and close to the attacked areas, which are either the grains or the grain boundaries as noted.

4.4. Stage D – local attack

The limited Na_2SO_4 cover on the surface is almost used up by the time acid fluxing becomes dominant. Apparently, little sulphur was observed in the Na_2WO_4-rich layer from EDS analysis shown in Fig. 5. It implied that sulphur had reacted with the substrate metal or escaped into the air. From a corrosion feature, namely the local attack of the grains and the grain boundaries as shown in Fig. 12, it is suggested that at this stage sulphur reacts with chromium to form CrS instead of NiS. This is inferred by the formation of the internal chromium-rich sulphides, as mentioned previously, which shows that CrS is more stable than NiS. Therefore, the selective sulphidation of chromium may occur. However, these sulphides would eventually oxidize due to oxygen penetrating through the porous layer from the free surface. In this reaction

$$2CrS + 3/2O_2 = Cr_2O_3 + 2S_{(diss)} \quad (29)$$

the released sulphur supplies the source for the consequent sulphidation. Spengler and Viswanathan [22] have shown that oxidation of internal chromium sulphides liberates sulphur which nucleates new sulphide particles along a front advancing into the alloy. This is confirmed by the results in this study shown in Figs 10 and 11. After these series reactions, the locally attacked areas of the grains and grain boundaries are transformed into chromium-rich oxides. The reactions are shown schematically in Fig. 13d.

Because grain boundaries are defect structures, they can accommodate more sulphur and can supply short-circuit paths for sulphur and oxygen as well. Therefore, in some attacked grain boundaries, the portions near the free surface are chromium-rich oxides, which are initially in the form of sulphides. However, grain boundaries further into the metal are chromium-rich sulphides from attack at the advancing sulphur front. It also has been observed that beside the grain boundaries of the chromium-rich oxides are chromium-rich sulphide particles, as shown in Fig. 11. It suggests that the originally chromium-rich sulphides growing in the grain boundaries are oxidized, and liberate sulphur which nucleates new sulphide particles inside grains.

The residual melt, rich in Na_2SO_4, penetrates through the porous scale, and acidic fluxing of Cr_2O_3 may occur

$$Cr_2O_3 = 2Cr^{3+} + 3O^{2-} \quad (30)$$

The acidic melt is achieved by WO_3 consuming oxygen to form WO_4^{2-} at this stage. The front areas of the dark attacked regions, as shown in Fig. 10, are WO_3 mixed with liquid phase which are tungsten-rich melt. Within the attacked region marked "F" in Fig. 10, some liquid-attacked areas are evident. It indicates that catastrophic corrosion results from the acidic fluxing, which is achieved by a refractory oxide of WO_3 stabilized as Na_2WO_4 but not by acidified Na_2SO_4, because almost no sulphur can be detected in the melt.

5. Conclusion

Immediately upon bringing the test discs to temperature, weight increase was due to the formation of chromium-rich oxides on the surface. Consequently, chromium-rich oxides and WO_3 were dissolved in molten Na_2SO_4 by basic fluxing. Only nickel-rich oxides survived and dispersed on the molten-phase surface. Na_2CrO_4 was a stable phase only in the basic melt. As the melt was acidified by continuously consuming oxygen ions, plate-like crystals of Cr_2O_3 were precipitated on the free surface by the conversion from Na_2CrO_4. The presence of sulphur suppressed the occurrence of selective oxidation of chromium and thereby prevented the formation of a protective Cr_2O_3-rich scale. Internal chromium-rich sulphide particles have been observed, instead of aluminium sulphides. This indicated that CrS is more stable than NiS. In some attacked grain boundaries, the upper portions were chromium-rich oxides, but the tips advancing into the alloy were chromium-rich sulphides. It is suggested that initially sulphur reacted with chromium to form CrS, as oxygen penetrating through the porous layer, CrS was oxidized into

Cr_2O_3 according to the reaction

$$2CrS + 3/2O_2 = Cr_2O_3 + 2S_{(diss)}$$

The liberated sulphur nucleated new chromium-rich sulphide particles along a front advancing into the alloy. There was indirect evidence to show that Na_2CrO_4 and Na_2WO_4 really existed within the scale. The melts at room temperature adsorbed water from humid air and recrystallized to form large Na_2CrO_4-rich or Na_2WO_4-rich crystals. The room-temperature crystalline morphology was subject to change after different exposure periods in air.

Acknowledgements

Many helpful discussions with Dr T. J. Rockett, Chemical Engineering Department, University of Rhode Island, are gratefully acknowledged. Provision of laboratory facilities in the Department of Chemical Engineering is also acknowledged.

References

1. P. S. SIDKY and M. G. HOCKING, *Corrosion Sci.* **27** (1987) 183.
2. *Idem., ibid.* **27** (1987) 205.
3. K. N. STRAFFORD and K. UPADHYA, paper presented at American Electrochemical Society, Detroit (October 1982).
4. C. J. ROSA, *Corrosion Sci.* **22** (1982) 1081.
5. V. VASANTASREE and M. G. HOCKING, *ibid.* **16** (1976) 261.
6. M. G. HOCKING and V. VASANTASREE, *ibid.* **16** (1976) 279.
7. A. DAVIN and D. COUTSOURADIS, *Cobalt* **19** (1963) 1.
8. N. BIRKS and G. H. MEIER, "Introduction to High Temperature Oxidation of Metals" (Arnold, London, 1983) pp. 141–44.
9. K. L. LUTHRA and D. A. SHORES, *J. Electrochem. Soc.* **127** (1980) 2202.
10. D. K. GUPTA and R. A. RAPP, *ibid.* **127** (1980) 2194.
11. A. K. MISRA, *ibid.* **133** (1986) 1029.
12. *Idem., ibid.* **133** (1986) 1038.
13. Y. S. ZHANG, *ibid.* **133** (1986) 655.
14. N. OTSUKA and R. RAPP, *ibid.* **137** (1990) 46.
15. *Idem., ibid.* **137** (1990) 53.
16. F. J. KOHL, G. J. SANTORO, C. A. STEARNS, G. C. FRYBURG and D. E. ROSNER, *ibid.* **126** (1979) 1054.
17. K. L. LUTHRA and H. S. SPACIL, *ibid.* **129** (1982) 649.
18. F. R. CHIEN and R. BROWN, *J. Mater. Sci.* **27** (1992) 1514.
19. G. C. FRYBURG, F. J. KOHL, C. A. STEARNS and W. L. FIELDER, *J. Electrochem. Soc.* **129** (1982) 571.
20. J. A. GOEBEL, F. S. PETTIT and G. W. GOWARD, *Metall. Trans.* **4** (1973) 261.
21. P. KOFSTAD, "High Temperature Corrosion" (Elsevier Applied Science, London, 1988) pp. 339, 362.
22. C. J. SPENGLER and R. VISWANATHAN, *Metall. Trans.* **3** (1972) 161.

Received 7 January
and accepted 13 May 1991